Characterization of Airborne Pathogen Transmission in Turbulent Molecular Communication Channels

Fatih Gulec*†, Falko Dressler†, Andrew W. Eckford*
* Department of Electrical Engineering and Computer Science, York University, Toronto, Ontario, Canada
Email: fgulec@yorku.ca, aeckford@yorku.ca
†School of Electrical Engineering and Computer Science, TU Berlin, Berlin, Germany
Email: dressler@ccs-labs.org

***Abstract*—Airborne pathogen transmission mechanisms play a key role in the spread of infectious diseases such as COVID-19. In this work, we propose a computational fluid dynamics (CFD) approach to model and statistically characterize airborne pathogen transmission via pathogen-laden particles in turbulent channels from a molecular communication viewpoint. To this end, turbulent flows induced by coughing and the turbulent dispersion of droplets and aerosols are modeled by using Reynolds-averaged Navier-Stokes equations coupled with realizable $k-\epsilon$ model and the discrete random walk model, respectively. Via the simulations realized by a CFD simulator, statistical data for the number of received particles are obtained. These data are post-processed to obtain the statistical characterization of the turbulent effect in the reception and to derive the probability of infection. Our results reveal that the turbulence has an irregular effect on the probability of infection which shows itself by the multi-modal distributions as a weighted sum of normal and Weibull distributions.**

I. Introduction

Airborne transmission is an important contagion mechanism of pathogens, e.g., viruses, bacteria, in the spread of infectious diseases such as influenza and COVID-19 [1]. In airborne transmission, infectious diseases spread by pathogen-laden particles such as droplets and aerosols through respiratory activities [2]. In the literature of fluid dynamics, computational fluid dynamics (CFD) simulators are widely employed to model airborne transmission via droplets in order to model turbulent flows and airflow-particle interactions more realistically. In [3], coughing and the dispersion of droplets are modeled by using the Navier-Stokes equations and large eddy simulation (LES) turbulence model. In [4] and [5], flows as a result of sneezing/coughing are modeled with Reynolds-averaged Navier-Stokes (RANS) equations coupled with the realizable $k-\epsilon$ and $k-\omega$ turbulence models, respectively.

The research in fluid dynamics literature focuses on the propagation of droplets after the emission but not the reception elaborately. However, there is a similarity between air-based molecular communication (MC) systems and airborne transmission of pathogens between two humans [6]–[8]. In addition, the transfer of pathogen-laden particles between humans can be considered as a way of communication [9]. Hence, the usage of MC is proposed to model the airborne transmission with a holistic approach [8], [10]–[15].

The studies in [8], [11] lay the theoretical and experimental foundations of dualities between pathogen-laden droplet propagation and MC. In [13] and [14], the transmission mechanism of Severe Acute Respiratory Syndrome-Corona Virus-2 in the respiratory system is modeled with a MC perspective. In [15], a statistical model for the spread of viruses through imperfectly fitted masks is proposed. In [10], an end-to-end MC system model which considers the coughed droplets as a cloud with a probabilistic approach is proposed to model the airborne transmission between two humans. This approach also enables an analytical derivation of infection probability which can be used in transmission and epidemiology models. However, none of the aforementioned works employs the turbulent flows and aerosols together with a MC perspective. Furthermore, the statistical characterization of received particles under turbulent flows and the corresponding expression for the probability of infection is not known.

In this paper, a CFD approach is proposed to model the airborne transmission of cough droplets and aerosols together with turbulent flows between an infectious and susceptible human which are the transmitter (TX) and receiver (RX), respectively. In this approach, the channel is modeled as a turbulent two-phase flow medium which comprises the movement of airflows with turbulence (continuous phase) and the motions of particles (discrete phase) interacting with these airflows and RX. The turbulence is modeled by employing the RANS equations coupled with the realizable $k-\epsilon$ model and the turbulent dispersion of particles is tracked in the CFD simulator by using the discrete random walk model.

In order to observe and characterize the effect of turbulence in airborne transmission, extensive CFD simulations are executed. Thus, statistical data for the received particles are obtained and employed to derive the probability of infection. Our statistical analysis shows that modeling the effect of turbulence on infections is not straightforward, since the probability density function of received particles are modeled by multi-modal distributions, i.e., weighted addition of normal and Weibull distributions. Lastly, it is shown that the increment

The work of Fatih Gulec was supported by German Academic Exchange Service (DAAD). The work of Falko Dressler was supported by the project MAMOKO funded by the German Federal Ministry of Education and Research (BMBF) under Grant 16KIS0917. Andrew W. Eckford was funded in part by a Discovery grant from the Natural Sciences and Engineering Research Council of Canada.

978-1-6654-3540-6/22 © 2022 IEEE

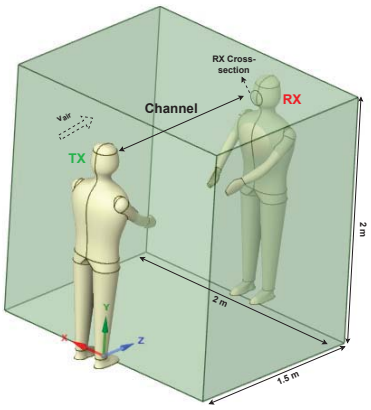

Fig. 1. Airborne pathogen transmission scenario between two humans.

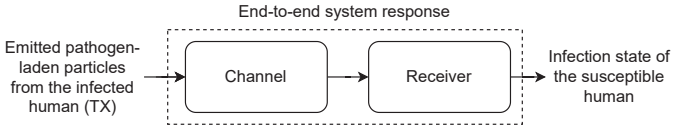

Fig. 2. End-to-end system model.

in the ambient airflow increases the probability of infection.

II. System Model

In this section, the system model for a scenario where the TX emits pathogen-laden spherical particles by coughing towards the RX in a room with an airflow as illustrated in Fig. 1 is detailed. As shown in Fig. 2, emitted particles from the TX is considered as an impulsive input signal and propagate through the channel and sensed by the RX. Hence, the end-to-end system response is given as the output of the system, i.e., the infection state of the susceptible human. The end-to-end system model includes the details about the receiver model, turbulent two-phase channel model and emitted particle characterization which is given as follows.

A. Emitted Pathogen-Laden Particle Size Distribution

In the literature of airborne transmission, only the propagation of large droplets ($\geq$ 10 μm) is taken into account. However, there is also evidence for the airborne transmission cases with aerosols ($<$ 10 μm) [1]. Therefore, aerosols are also included to the emitted cough particles in our scenario. Experimental data in [16], [17] are used for the number and size (diameter) of spherical droplets and aerosols, respectively. These data are fitted by using the maximum likelihood estimation for a better implementation in the CFD simulator according to a Weibull distribution which has the probability density function (pdf) for data samples ($x \geq 0$) as given by

$$f(x) = \frac{k}{\lambda}\left(\frac{x}{\lambda}\right)^{k-1} \mathrm{e}^{-\left(\frac{x}{\lambda}\right)^{k}}, \tag{1}$$

where k and λ are shape and scale parameters, respectively. These parameters are estimated by using the maximum likelihood estimation which is based on finding the unknown parameter values ($\mathbf{y} = [y_1, y_2, ..., y_n]^T$) which maximizes the log likelihood function ($\mathcal{L}_n(\mathbf{y}; \mathbf{x})$) as given by [18]

$$\mathcal{L}_n(\mathbf{y}; \mathbf{x}) = \log\left[f_n(\mathbf{x}; \mathbf{y})\right] = \sum_{k=1}^{n} \log\left[f_k(x_k; \mathbf{y})\right], \tag{2}$$

where $\mathbf{x}$ represents the observed data samples, $\log(.)$ is the natural logarithm, and $f_k(x_k; \mathbf{y})$ is the joint pdf where data samples are assumed as independent and identically distributed random variables. Hence, the estimated parameters are determined according to the rule as given below:

$$\hat{\mathbf{y}} = \arg\max_{\mathbf{y} \in \Theta} \mathcal{L}_n(\mathbf{y}; \mathbf{x}) \tag{3}$$

where Θ is the parameter space. By applying this rule, the parameters are estimated in a least-square sense iteratively, i.e., the best fit for the estimated function is found by minimizing the sum of the squared error between the estimated values and actual values. Thus, the shape and scale parameters for the pdfs of droplet (k_d, λ_d) and aerosol sizes (k_a, λ_a) are estimated as $\lambda_d = 0.0001184$ with the estimation variance $5.553\mathrm{e}-12$, $k_d = 1.9368$ with the estimation variance 0.00293, and $\lambda_a = 7.92\mathrm{e}-7$ with the estimation variance $5.0147\mathrm{e}-18$, $k_a = 1.7338$ with the estimation variance $2.785\mathrm{e}-5$, respectively.

B. Turbulent Two-Phase Flow Channel Model

Pathogen-laden particles, which consist of large droplets and aerosols, are subject to some interactions with the air after the emission with an initial velocity from the TX. These interactions lead to turbulent airflows in the vicinity of the TX in addition to the constant air velocity (v_{air}). The motion of particles rely on these airflows as well as other factors such as gravity and air drag. All of these motions in the MC channel can be examined as continuous (or gas) phase for airflows and discrete (or liquid) phase for particle movements.

1) Continuous Phase: Turbulence is considered by using 3-D Navier-Stokes equations that determine airflow velocity components u_i where $i = 1, 2, 3$ for x, y and z in Cartesian coordinates, respectively. To reduce the computational complexity for the solution of Navier-Stokes equations, RANS equations, which average Navier-Stokes equations, are employed [19]. Instantaneous flow velocities are considered as the addition of the average values ($\overline{u_i}$) and the fluctuation values (u_i'), i.e., $u_i = \overline{u_i} + u_i'$. RANS equations in tensor form for the average velocities are given by [20]

$$\frac{\partial \rho}{\partial t} + \frac{\partial}{\partial x_i}(\rho \overline{u_i}) = 0 \tag{4}$$

$$\frac{\partial \rho}{\partial t}(\rho \overline{u_i}) + \frac{\partial}{\partial x_j}(\rho \overline{u_i u_j}) = -\frac{\partial p}{\partial x_i} + \frac{\partial}{\partial x_j}\left[\mu\left(\frac{\partial \overline{u_i}}{\partial x_j} + \frac{\partial \overline{u_j}}{\partial x_i}\right) - \frac{2}{3}\delta_{ij}\frac{\partial \overline{u_k}}{\partial x_k}\right] + \frac{\partial\left(-\rho \overline{u_i' u_j'}\right)}{\partial x_j}, \tag{5}$$

where ρ is the fluid density, μ is the dynamic viscosity, p is the fluid pressure, and δ_{ij} is the Kronecker delta function and x_i shows the Cartesian coordinates. In (5), the terms $-\rho \overline{u_i' u_j'}$

give the Reynolds stresses calculated by using the Boussinesq hypothesis to close RANS equations as given by [19] [21]

$$-\rho\overline{u_i'u_j'} = \mu_t\left(\frac{\partial\overline{u_i}}{\partial x_j}+\frac{\partial\overline{u_j}}{\partial x_i}\right)-\frac{2}{3}\left(\rho k+\mu_t\frac{\partial\overline{u_k}}{\partial x_k}\right) \quad (6)$$

where μ_t is the turbulent viscosity and k is the turbulent kinetic energy. Here, k and its dissipation rate (ϵ) are obtained by the realizable $k-\epsilon$ model which is a widely used and accurate turbulence model as applied in [4]. Although LES model is more accurate than $k-\epsilon$ model, it is computationally very complex and not appropriate for our aim which is to obtain statistical data by running several simulations. Transport equations for realizable $k-\epsilon$ model are given by [22]

$$\frac{\partial(\rho k)}{\partial t}+\frac{\partial(\rho k u_j)}{\partial x_j}=\frac{\partial}{\partial x_j}\left[\left(\mu+\frac{\mu_t}{\sigma_k}\right)\frac{\partial k}{\partial x_j}\right]+G_k-\rho\epsilon+S_k \quad (7)$$

$$\frac{\partial(\rho\epsilon)}{\partial t}+\frac{\partial(\rho\epsilon u_j)}{\partial x_j}=\frac{\partial}{\partial x_j}\left[\left(\mu+\frac{\mu_t}{\sigma_\epsilon}\right)\frac{\partial\epsilon}{\partial x_j}\right]+\rho C_1 S\epsilon - \rho C_2\frac{\epsilon^2}{k+\sqrt{\nu\epsilon}}+S_\epsilon, \quad (8)$$

where $C_1=\max\left[0.43,\frac{\eta}{\eta+5}\right]$, $\eta=Sk/\epsilon$, and $S=\sqrt{2S_{ij}S_{ij}}$, S_k and S_ϵ are user-defined source terms, $C_2=1.9$, $C_{1\epsilon}=1.44$, $\sigma_k=1$ and $\sigma_\epsilon=1.2$ are the turbulent Prandtl numbers for k and ϵ, respectively. Here, G_k which is the term related with the turbulent kinetic energy is given as $G_k=\mu_t S^2$ with μ_t as given by

$$\mu_t=\rho C_\mu\frac{k^2}{\epsilon} \quad (9)$$

where C_μ is calculated by the formulas given in [22] (equations (19)-(21) in [22]).

By solving the equations (4)-(9) iteratively, the average airflow velocities can be obtained whereas the fluctuating airflow velocities are calculated in stochastic tracking of particles during the turbulent dispersion as follows.

2) Discrete Phase: According to the Newton's second law of motion, the acting forces on a spherical particle is given by

$$m_p\frac{d\overrightarrow{u_p}}{dt}=m_p\frac{\overrightarrow{u}-\overrightarrow{u_p}}{\tau_r}+m_p\frac{\overrightarrow{g}(\rho_p-\rho)}{\rho_p}, \quad (10)$$

where m_p shows the particle mass, ρ_p is the particle density, $\overrightarrow{u}$ and $\overrightarrow{u_p}$ are the air and particle velocities, respectively. Here, the second term on the right hand side shows the net force downwards (difference between gravitational and buoyant force) as also derived in [10], and the first term on the right hand side gives the drag force where $\tau_r=(24\rho_p d_p^2)/(18\mu C_D Re)$ is the particle relaxation time [23], Re is the Reynolds number, d_p is the particle diameter. C_D is the drag coefficient following the spherical drag law as given by [24]

$$C_D=K_1+\frac{K_2}{Re}+\frac{K_3}{Re^2} \quad (11)$$

where K_1, K_2 and K_3 are experimentally validated constants which change according to Re as given in [24].

It should be noted that a constant airflow velocity (v_{air}) is added to $\overrightarrow{u}$ in the $+z$ direction towards the RX in addition to the turbulent airflow velocity as also shown in Fig. 1. The stochastic effect of turbulence is incorporated to the system model by adding the fluctuation values, i.e., u_i', via the discrete random walk (DRW) model so that the turbulent dispersion of particles are modeled. According to DRW model, u_i' is determined as [25] [21]

$$u_i'=\beta\sqrt{\frac{2k}{3}} \quad (12)$$

where β is a standard normal random variable, i.e., $\beta=\mathcal{N}(0,1)$. Each particle is tracked along the eddy interaction time as given by $t_{int}=\min(\tau_e,t_R)$ where τ_e is the eddy lifetime in a turbulent flow and calculated by $\tau_e=-T_L\ln(r)$ where r is a standard uniform random variable and $T_L\approx 0.15k/\epsilon$ is the Lagrangian integral time. In addition, t_R is the particle eddy transit (or crossing) time as given by

$$t_R=-\tau_r\ln\left[1-\left(\frac{L_e}{\tau_r|\overrightarrow{u}-\overrightarrow{u_p}|}\right)\right], \quad (13)$$

where L_e is the eddy length scale. A new value is assigned to u_i' via updating β, when t_{int} is reached during the tracking of a particle.

C. Receiver Model

As for the reception, particles reaching at the RX cross-section as shown in Fig. 1 are counted until every particle leaves the flow domain. This RX cross-section is in the center of the human face including eyes, nose and the mouth and is a circle having a diameter $r_R=(\sqrt{\beta_{bb}^2+\beta_{ss}^2})/2$ where β_{bb} is the biocular breadth and β_{ss} is the Sellion-Stomion length as also given in [10]. Next, the usage of the models by numerically solving the equations in this section in a CFD simulator is elaborated.

III. Computational Fluid Dynamics Simulator

In this section, the details about the setup of CFD simulations which are executed by using Ansys Fluent 2021 R.2 simulator are given. As shown in Fig. 1, two identical manikins are used as the TX and RX which are 176 cm high. The flow domain which is shown as a green cuboid has the 3-D dimensions $2\times 2\times 1.5$ m. The airflow and particle motions are simulated within this flow domain which includes the TX emission and RX reception surfaces. The CFD simulator calculates variables such as pressure and velocity with the finite volume method which requires the flow domain to be divided into small volumes. To this end, meshing is performed by generating 74520, 25772 and 26092 tetrahedral cells for the flow domain, TX and RX volumes, respectively.

The mouth of the TX is modeled as an ellipse (4×1 cm, area $=314\text{mm}^2$) [3] and aligned in the same axis with the RX. The center of the RX cross-section and TX are at a height of 162.6 cm and 159 cm high from the ground, respectively. Particles and air are emitted with an initial velocity (u_0) from this mouth surface along the emission time (T_e) according to the size distributions derived in Section II-A. In the flow domain, boundary conditions are arranged so that particles can

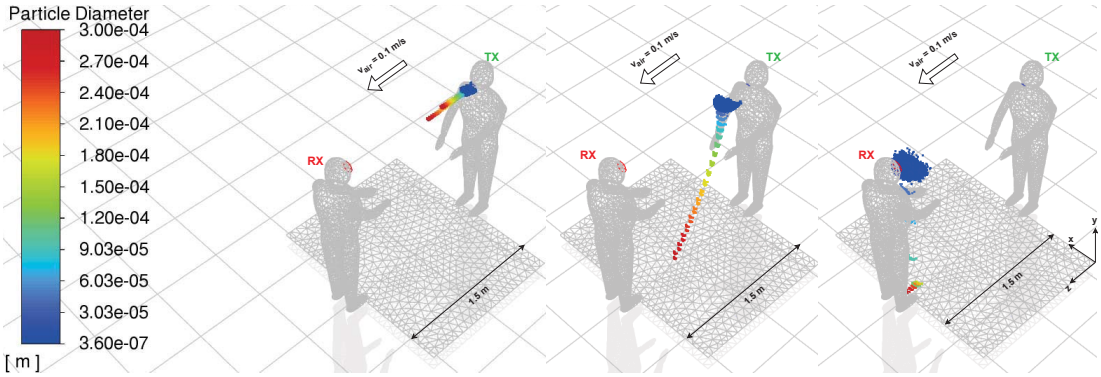

Fig. 3. Visualization of a human cough and its reception with 48800 particles for $v_{air} = 0.1$ m/s at (a) $t = 0.12$ s (b) $t = 1.5$ s (c) $t = 12$ s.

escape at the end of the flow domain's surface and particles are absorbed at the RX circular cross-section. Other surfaces are configured as reflective for particles. By using these boundary conditions and the governing equations (4)-(8), the CFD simulator discretize these equations by converting them from their integral form to algebraic equations relating p and $\overline{u_i}$ values at each cell center [21]. Then, these equations are linearized via Taylor series expansions and solved iteratively by guessing the pressure and velocity values at each cell center after each iteration. At each iteration, the mass conservation is calculated and iterations continue until the error of mass imbalance converges. In Ansys Fluent, the coupled pressure-based solver is used for the calculations of transient simulations. After $\overline{u_i}$ is determined for each cell at each time step (Δt), these values are used by also using the models explained in Section II-B2 to calculate the turbulent dispersion of particles (including their interactions with continuous phase), i.e., their instantaneous velocities and positions.

IV. Simulation Results

In this section, visual simulation results which are obtained via the CFD simulator as detailed in Section III are presented. The CFD simulations are repeated 500 times for each of three different air velocities, i.e., $v_{air} = \{0.1, 0.3, 0.5\}$ m/s using the parameter values in Table I along t_s. The initial cough flow rates for droplets (Q_d) and aerosols (Q_a) are calculated by dividing the emitted droplet and aerosol masses to T_e. The number of emitted number of droplets (10 μm - 300 μm) and aerosols (0.36 μm - 9.5 μm) are configured accordingly with the values in Section II-A. In addition, β_{bb} and β_{ss} values are taken as the average value of female and male values to calculate r_R of the RX as also applied in [10].

TABLE I
Simulation Parameters

Parameter	Value	Parameter	Value
Δt	0.06 s	t_s	$\{18, 9, 6\}$ s
T_e	0.12 s [26]	u_0	11.2 m/s (cough) [27]
Q_d	$47.83 \times 10^{-}6$ kg/s [16]	g	9.81 m/s^2
Q_a	9.9259 kg/s [17]	μ	$17.894{\times}10^{-6}$ kg/(m s)
ρ	1.225 kg/m^3	β_{bb} (female)	8.853 cm [28]
ρ_p	998.2 kg/m^3	β_{bb} (male)	9.131 cm [28]
N_d	800	β_{ss} (female)	6.901 cm [28]
N_a	48000	β_{ss} (male)	7.57 cm [28]

In Fig. 3, the trajectory and dispersion of the cough particles can be observed for $v_{air} = 0.1$ m/s between the emission and reception. At the initial state, larger particles tend to move faster due to the initial velocity as shown in Fig. 3 (a). However, as these larger particles (or large droplets) continue their movement, they are affected by the air drag and lose their momentum more quickly. In addition, large droplets fall down to the ground due to the gravity as it is clearly observed in Fig. 3 (b). In contrast to large droplets, aerosols are affected less by the gravity and air drag due to their small sizes. Therefore, they are entrained by the ambient air flow towards the RX and large droplets cannot reach at the RX for a distance of 1.5 m. Furthermore, the effect of ambient air velocity on the dispersion of particles is shown in Fig. 4. These results show that as v_{air} increases, particles propagate for a longer distance before they fall down to the ground. Besides, smaller v_{air} causes more dispersion on the particles as shown in Fig. 4 (a)-(c), while it increases the reception time of droplets. The reason of this dispersion is the randomness due to the effect of turbulence at the initial state of the particle propagation. In the next section, data obtained via CFD simulations are used for the statistical characterization of the probability of infection.

V. Probability of Infection

In this section, the collected data for the received number of particles via the CFD simulations are analyzed and employed for statistical characterization of the reception in airborne pathogen transmission. Then, the probability of infection is derived for different scenarios by using these statistics.

In Fig. 5, the histograms and the fitted probability density functions (pdfs) of the received number of particles for three different ambient air velocities are given. As observed from this figure, the distributions are multi-modal and can be modeled by using the weighted sums of different distributions. To this end, these weighted distributions are determined visually

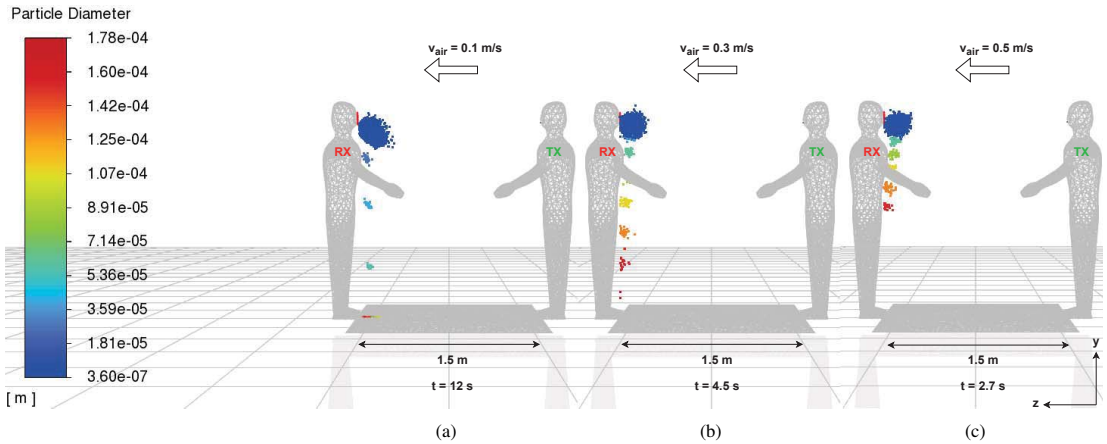

Fig. 4. The effect of different air velocities and turbulence on the pathogen-laden cough particles during the reception for (a) $v_{air} = 0.1$ m/s at $t = 12$ s (b) $v_{air} = 0.3$ m/s at $t = 4.5$ s (c) $v_{air} = 0.5$ m/s at $t = 2.7$ s.

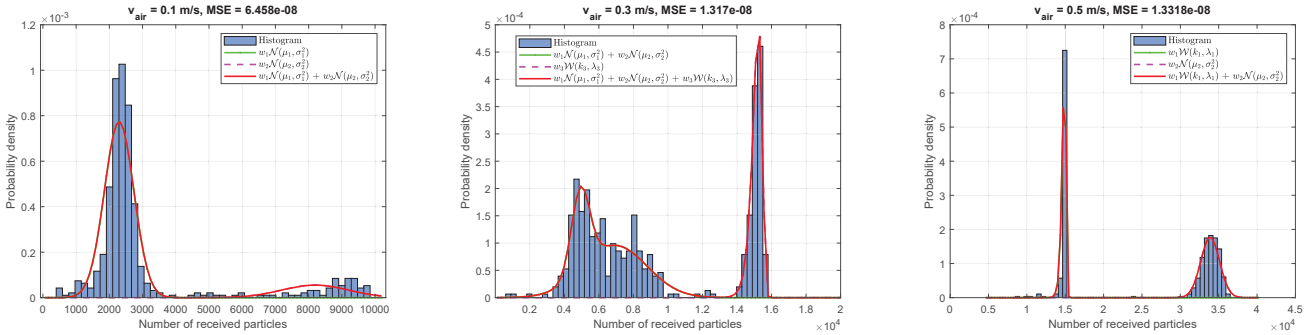

Fig. 5. Probability density function of N_R for (a) $v_{air} = 0.1$ m/s (b) $v_{air} = 0.3$ m/s (c) $v_{air} = 0.5$ m/s.

according to the shapes of histograms, which are given as

$$f_{N_{R_1}}(N_R) = w_1\mathcal{N}(\mu_1, \sigma_1^2) + w_2\mathcal{N}(\mu_2, \sigma_2^2) \quad (14)$$

$$f_{N_{R_2}}(N_R) = w_1\mathcal{N}(\mu_1, \sigma_1^2) + w_2\mathcal{N}(\mu_2, \sigma_2^2) + w_3\mathcal{W}(k_3, \lambda_3) \quad (15)$$

$$f_{N_{R_3}}(N_R) = w_1\mathcal{W}(k_1, \lambda_1) + w_2\mathcal{N}(\mu_2, \sigma_2^2), \quad (16)$$

where w_1, w_2 and w_3 show the weights, $\mathcal{N}(\mu_R, \sigma_R^2)$ is the normal distribution with mean μ_R and variance σ_R^2, $\mathcal{W}(k_R, \lambda_R)$ is the Weibull distribution with the scale parameter λ_R and shape parameter k_R, and $f_{N_{R_1}}(N_R)$, $f_{N_{R_2}}(N_R)$, $f_{N_{R_3}}(N_R)$ are the pdfs for $v_{air} = 0.1$ m/s, $v_{air} = 0.3$ m/s, and $v_{air} = 0.5$ m/s, respectively. The parameters given in (14)-(16) are estimated as given in Table II via the maximum likelihood estimation method detailed in Section II-A.

In the next step, these derived pdfs in (14)-(16) with their estimated parameters given in Table II can be employed to obtain the probability of infection (P_{inf}) as given by [10]

$$P_{inf_i} = P(N_R > \gamma) = \int_{\gamma}^{\infty} f_{N_{R_i}}(x)dx \quad (17)$$

where i shows the index according to v_{air} as also applied in (14)-(16) and γ is the detection threshold corresponding to the immune system's strength of the RX. Thus, the derived expressions for the probability of infections for different air velocities are given by

$$P_{inf_1} = w_1 Q\left(\frac{\gamma - \mu_1}{\sigma_1}\right) + w_2 Q\left(\frac{\gamma - \mu_2}{\sigma_2}\right) \quad (18)$$

$$P_{inf_2} = w_1 Q\left(\frac{\gamma - \mu_1}{\sigma_1}\right) + w_2 Q\left(\frac{\gamma - \mu_2}{\sigma_2}\right) + w_3 e^{-\left(\frac{\gamma}{\lambda_3}\right)^{k_3}} \quad (19)$$

$$P_{inf_3} = w_1 e^{-\frac{\gamma}{\lambda_1}^{k_1}} + w_2 Q\left(\frac{\gamma - \mu_2}{\sigma_2}\right), \quad (20)$$

where $Q(x) = \frac{1}{\sqrt{2\pi}} \int_x^{\infty} \mathrm{e}^{-\frac{u^2}{2}} du$ shows the Q-function. The resulting plot for these P_{inf} values given in (18)-(20) for different γ values are shown in Fig. 6. These results show that larger air velocities increase the infection probability for susceptible people for a face-to-face scenario. Even though the immune system's strength of a susceptible human is high, the risk for infection still continues due to the higher exposure of pathogen-laden particles. The results in Fig. 6 also show the effect of aerosols which are not taken into account before in the literature for the calculation of the probability of infection in addition to the effect of large droplets in smaller numbers. This derivation of P_{inf} shows that the modeling the reception of particles is non-trivial due to the highly complex nature of turbulence and it shows that multi-modal distributions lie un-

TABLE II
ESTIMATED STATISTICAL PARAMETERS

Pdf	w_1	Distribution 1		w_2	Distribution 2		w_3	Distribution 3		MSE
$f_{N_{R_1}}$	0.86	μ_1=2294.9	σ_1=444.2	0.14	μ_2=8195.7	σ_2=1000	-	-	-	6.458e−8
$f_{N_{R_2}}$	0.20	μ_1=4938.1	σ_1=527.5	0.44	μ_2=6929.5	σ_2=1846.1	0.36	k_3=58.4	λ_3=15242.7	1.317e−8
$f_{N_{R_3}}$	0.46	k_1=60.9	λ_1=14915.6	0.54	μ_2=33888.1	σ_2=1218.8	-	-	-	1.332e−8

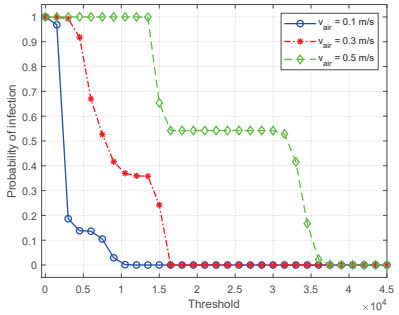

Fig. 6. Probability of infection according to γ for different v_{air} values.

der this turbulent complexity. These analytical derivations also can be employed in epidemiology studies with more realistic parameters for interhuman airborne pathogen transmission.

VI. CONCLUSION

In this paper, the airborne transmission of pathogens emitted via coughing between two humans is modeled with a CFD approach incorporating turbulent airflows and turbulent dispersion of droplets and aerosols. By using the statistical data collected with CFD simulations, it is revealed that turbulence cause multi-modal distributions for the pdf of received particles by the susceptible human. Furthermore, numerical results show that augmented air velocity causes the increment of the probability of infection. Derived probability of infection expressions can be employed in epidemiological models to realistically consider the indoor airborne transmission. As the future work, it is planned to extend this study by including scenarios with masks and breathing.

REFERENCES

[1] G. Seminara, B. Carli, G. Forni, S. Fuzzi, A. Mazzino, and A. Rinaldo, "Biological fluid dynamics of airborne covid-19 infection," *Rendiconti Lincei. Scienze fisiche e naturali*, vol. 31, no. 3, pp. 505–537, 2020.

[2] R. Mittal, R. Ni, and J.-H. Seo, "The flow physics of covid-19," *J. of fluid Mechanics*, vol. 894, 2020.

[3] M.-R. Pendar and J. C. Páscoa, "Numerical modeling of the distribution of virus carrying saliva droplets during sneeze and cough," *Phys. of Fluids*, vol. 32, no. 8, p. 083305, 2020.

[4] G. Busco, S. R. Yang, J. Seo, and Y. A. Hassan, "Sneezing and asymptomatic virus transmission," *Phys. of Fluids*, vol. 32, no. 7, p. 073309, 2020.

[5] T. Dbouk and D. Drikakis, "On coughing and airborne droplet transmission to humans," *Phys. of Fluids*, vol. 32, no. 5, p. 053310, 2020.

[6] F. Gulec and B. Atakan, "Fluid dynamics-based distance estimation algorithm for macroscale molecular communication," *Nano Commun. Netw.*, vol. 28, p. 100351, 2021.

[7] F. Gulec and B. Atakan, "A droplet-based signal reconstruction approach to channel modeling in molecular communication," *IEEE Trans. Mol. Biol. Multi-Scale Commun.*, vol. 7, no. 1, pp. 64–68, 2021.

[8] M. Schurwanz, P. A. Hoeher, S. Bhattacharjee, M. Damrath, L. Stratmann, and F. Dressler, "Duality between coronavirus transmission and air-based macroscopic molecular communication," *IEEE Trans. Mol. Biol. Multi-Scale Commun.*, vol. 7, no. 3, pp. 200–208, 2021.

[9] M. Khalid, O. Amin, S. Ahmed, B. Shihada, and M.-S. Alouini, "Communication through breath: Aerosol transmission," *IEEE Commun. Mag.*, vol. 57, no. 2, pp. 33–39, 2019.

[10] F. Gulec and B. Atakan, "A molecular communication perspective on airborne pathogen transmission and reception via droplets generated by coughing and sneezing," *IEEE Trans. Mol. Biol. Multi-Scale Commun.*, vol. 7, no. 3, pp. 175–184, 2021.

[11] M. Schurwanz, P. Hoeher, S. Bhattacharjee, M. Damrath, L. Stratmann, and F. Dressler, "Infectious disease transmission via aerosol propagation from a molecular communication perspective: Shannon meets coronavirus," *IEEE Commun. Mag.*, vol. 59, no. 5, pp. 40–46, 2021.

[12] M. T. Barros *et al.*, "Molecular communications in viral infections research: Modelling, experimental data and future directions," *IEEE Trans. Mol. Biol. Multi-Scale Commun.*, vol. 7, no. 3, pp. 121–141, 2021.

[13] C. Koca, M. Civas, S. M. Sahin, O. Ergonul, and O. B. Akan, "Molecular communication theoretical modeling and analysis of sars-cov2 transmission in human respiratory system," *IEEE Trans. Mol. Biol. Multi-Scale Commun.*, vol. 7, no. 3, pp. 153–164, 2021.

[14] S. Pal, N. Islam, and S. Misra, "Vivid: In vivo end-to-end molecular communication model for covid-19," *IEEE Trans. Mol. Biol. Multi-Scale Commun.*, vol. 7, no. 3, pp. 142–152, 2021.

[15] S. Lotter, L. Brand, M. Schäfer, and R. Schober, "Statistical modeling of airborne virus transmission through imperfectly fitted face masks," in *Proc. ACM Int. Conf. Nanoscale Comput. and Commun.*, 2021, pp. 1–7.

[16] X. Xie, Y. Li, H. Sun, and L. Liu, "Exhaled droplets due to talking and coughing," *J. of the Roy. Soc. Interface*, vol. 6, no. suppl_6, pp. S703–S714, 2009.

[17] W. G. Lindsley *et al.*, "Quantity and size distribution of cough-generated aerosol particles produced by influenza patients during and after illness," *J. of occupat. and environ. hygiene*, vol. 9, no. 7, pp. 443–449, 2012.

[18] A. Papoulis and S. U. Pillai, *Probability, random variables, and stochastic processes*. Tata McGraw-Hill Education, 2002.

[19] T. Cebeci, J. P. Shao, F. Kafyeke, and E. Laurendeau, *Computational fluid dynamics for engineers: from panel to Navier-Stokes methods with computer programs*. Springer, 2005.

[20] R. Bi, S. Ali, E. Savory, and C. Zhang, "A numerical modelling investigation of the development of a human cough jet," *Eng. Computations*, 2021.

[21] A. FLUENT, "12.0 theory guide-1.2," 2021.

[22] T.-H. Shih, W. W. Liou, A. Shabbir, Z. Yang, and J. Zhu, "A new k-ϵ eddy viscosity model for high reynolds number turbulent flows," *Computers & fluids*, vol. 24, no. 3, pp. 227–238, 1995.

[23] R. G. Gordon, "Error bounds in equilibrium statistical mechanics," *J. of Math. Phys.*, vol. 9, no. 5, pp. 655–663, 1968.

[24] S. Morsi and A. Alexander, "An investigation of particle trajectories in two-phase flow systems," *J. of Fluid Mechanics*, vol. 55, no. 2, pp. 193–208, 1972.

[25] A. A. Mofakham and G. Ahmadi, "Improved discrete random walk stochastic model for simulating particle dispersion and deposition in inhomogeneous turbulent flows," *J. of Fluids Eng.*, vol. 142, no. 10, 2020.

[26] B. Scharfman, A. Techet, J. Bush, and L. Bourouiba, "Visualization of sneeze ejecta: steps of fluid fragmentation leading to respiratory droplets," *Experiments in Fluids*, vol. 57, no. 2, pp. 1–9, 2016.

[27] S. Zhu, S. Kato, and J.-H. Yang, "Study on transport characteristics of saliva droplets produced by coughing in a calm indoor environment," *Building and environment*, vol. 41, no. 12, pp. 1691–1702, 2006.

[28] J. W. Young *et al.*, "Head and face anthropometry of adult us civilians," Civil Aerospace Medical Institute, Tech. Rep., 1993.